## Findings

Findings for the 5 different sub-projects of this work are described as follows:

Subproject 1) Simulation of fluid flow and pressure distribution in metal delivery system in single-roll spin-casting of aluminum

A computational model has been developed of turbulent fluid flow and pressure distribution in the aluminum strip-casting apparatus at Cornell University. The model solves the Navier Stokes equations using the standard k-e turbulence model in a computational domain that includes the entire metal delivery system, including the puddle region. A special boundary condition at the solidification front enforces mass transfer across the liquid / solid interface according to the strip velocity. Several different models were investigated to handle the free surface of the liquid pool. These included fixed geometry (where the shape of the liquid pool was prescribed) and free-surface model computations, where the shape of the free surface was calculated using the two-phase Volume-of-Fluid method. The latter model included the effects of surface tension, and is the more accurate model. The equations are solved with the commercial package FLUENT on a very fine finite-difference grid which featured 50 cells through the thickness of the puddle. The geometry and casting conditions are for case 43, taken from [1], and are given in the Findings section. The problem presented computational challenges, including both accuracy and convergence difficulties, which were addressed in sub-project 2.

The model has revealed that pressure drops linearly in the upper regions of the metal delivery system according to the metallostatic head. The highest pressure gradient is found within the liquid pool just beneath the thin slit that delivers molten metal into the puddle on the wheel. Pressure drops significantly within the puddle, owing to the high surface tension on its edges, which curve to balance the high internal pressure. Pressure in this region is nonlinear, as it is affected also by the velocity gradients. The rapid acceleration of the strip causes a pressure drop towards the downstream region of the puddle, which might contribute to the variations in the strip thickness.

Work with test problems (subproject 2) has revealed that the K-e model of turbulence used in the simulation over-predicts the pressure drop along a channel with flowing fluid, relative to the exact solution obtained with a direct numerical simulation using a new code on a GPU processing system. Because the pressure drop in the model is forced to match the physical process, the shape of the puddle is much shorter and compact than observed experimentally. Improvements to the turbulence model are needed to obtain a better quantitative match with the experiments, but the qualitative behaviors are all logical and shed significant new light on the process.

This pressure is important because it controls the fluid flow, and its fluctuations are suspected to cause most of the observed defects in the strip product.

Sample results from the computational model reveal the pressure distribution in the strip-casting process at Cornell. The computational domain is given in Fig. 1.1, and is based on case 43 in Refs. 1.1-1.3, which provide details of the test conditions. The pressure contours calculated using the fixed-domain model are shown in Fig. 1.2, velocity and pressure contours from the VOF model in Fig. 1.3, and pressure distribution along vertical and horizontal sections in Figs. 1.3 and 1.4.

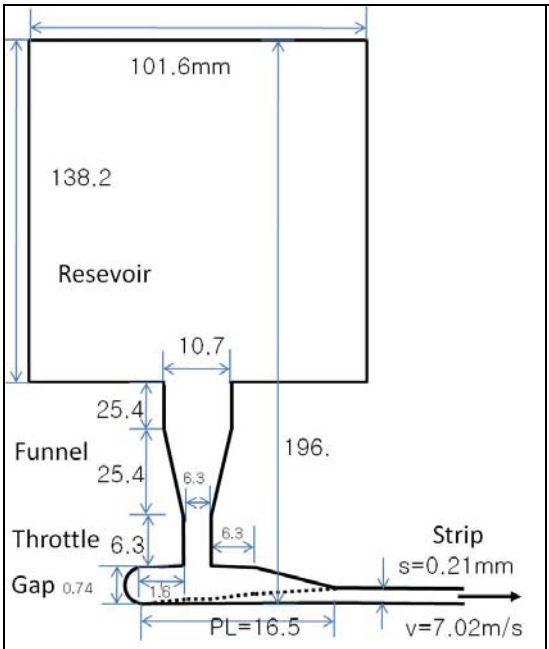


Fig. 1.1 Geometry of metal delivery system and computational domain

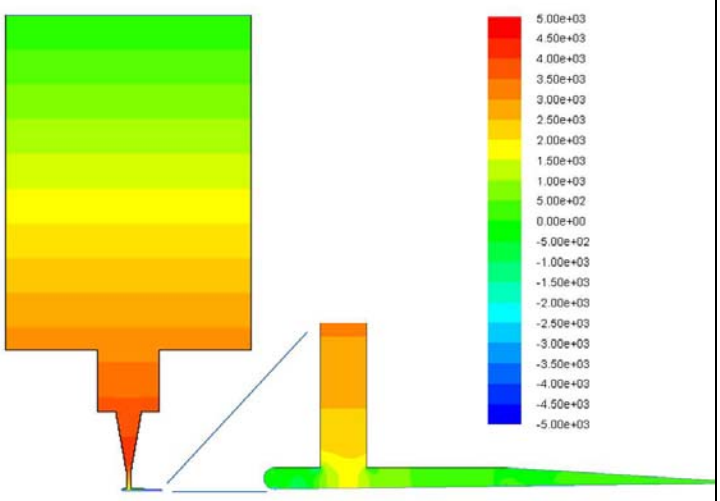


Fig. 1.2. Pressure contours (Pa) in the metal delivery system, with close-up of the puddle region (fixed domain model)

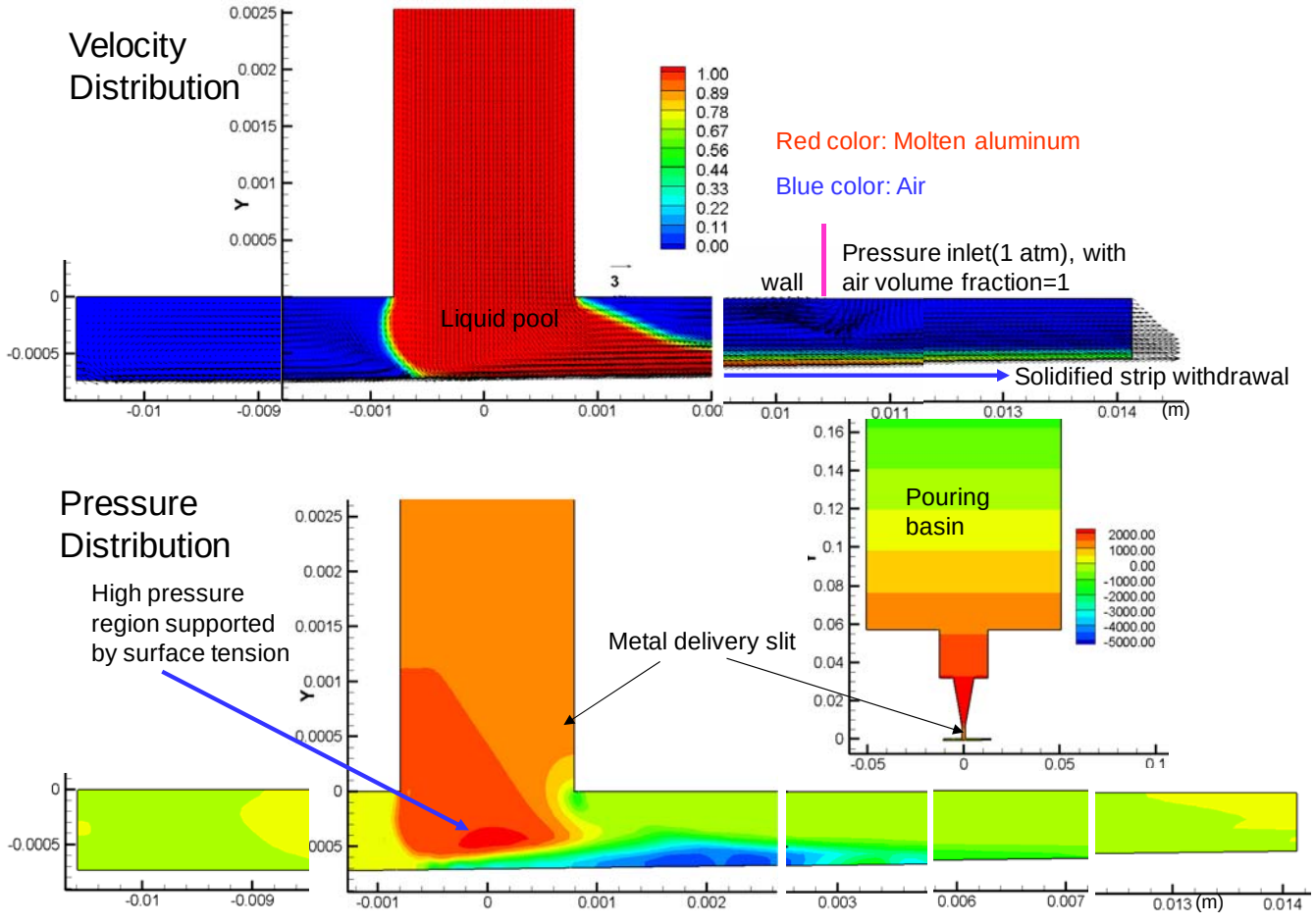


Fig. 1.3 – Velocity and pressure distribution computed in liquid pool of melt-spinning process using computational model of turbulent fluid flow with VOF method, showing calculated shape of liquid puddle, featuring curved surfaces supported by surface tension, and steep pressure gradients in the liquid pool near the accelerating strip.

The pressure increases linearly from atmospheric pressure (0 gage pressure) at the top surface of the reservoir to a maximum found near the bottom of the funnel, as shown clearly in Fig. 1.4. This pressure matches the classic simple analytical solution for hydrostatic pressure above this point, as the velocity (kinetic energy) terms in the Bernoulli equation are small. Below this point of maximum flow constriction, pressure drops as the liquid feeds the puddle, which effectively "pulls" liquid down from the delivery slit or "throttle" region. The thickness of this thin slit that comprises the bottom of the funnel region governs the liquid flow rate, which in turn governs the thickness of the final product.

Simple hydrostatic pressure governs the distribution in the reservoir and funnel region that delivers molten metal into the puddle. Contours are horizontal until the inside of the puddle region just below the throttle slit. Figure 1.5 shows that the maximum pressure in the puddle region is found just below the throttle, where downward flowing liquid impacts the solidification front, (causing a thinning of solidifying strip, as shown elsewhere in this project). At the left free surface of the puddle, surface tension forces generate a cylindrical shape, which balances the internal pressure at a significant level and thereby supports the puddle. The pressure of 2400 Pa computed here matches the simple analytical solution for surface tension with 0.37mm radius of curvature. Pressure drops towards the right side of the puddle, reaching atmospheric pressure (0 Pa gage) along the sloping, flat right boundary.

The calculated pressure variations, (including the slight negative pressure at one point) are believed to be numerical errors. The oscillating pressure caused by surface tension forces which are expected to be generated when this boundary fluctuates due to the turbulent flow is ignored in this time-averaged model. This work shows that the surface tension in the left meniscus, which is governed by the instantaneous curvature of the liquid pool in this region, has a very important effect on the entire process. Minor variations in free surface shape cause changes in meniscus curvature, and generate corresponding pressure fluctuations in the puddle. This causes oscillations in the liquid pool which govern the initial solidification and surface quality of the final strip. Pressure fluctuations are also expected due to variations in the location of the transition between laminar and turbulent flow, (Re ~5,000), which was not considered in this study.

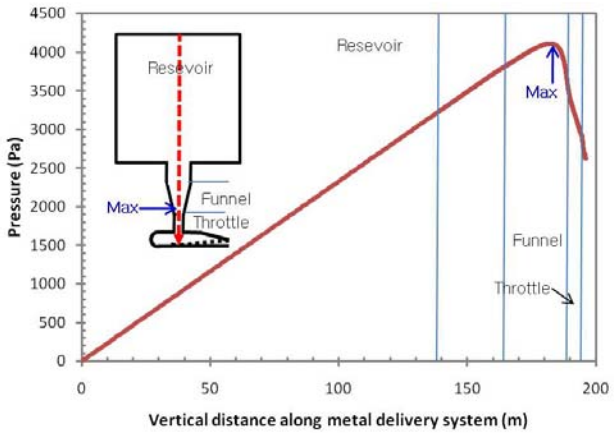


Fig. 1.4 Pressure distribution along vertical axis of the system

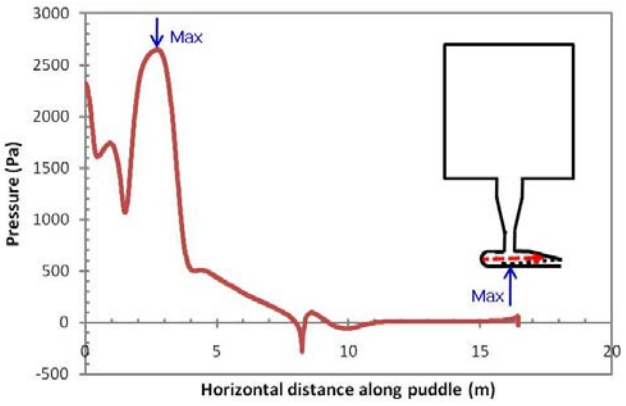


Fig. 1.5 Pressure distribution along horizontal axis along the center of the liquid puddle


1.1 A. Sundararajan, B. G. Thomas, J. Sengupta, Heat Transfer during Melt Spinning of Al-7%Si Allo y on a Cu-Be Wheel ", 2007, table 2, p. 21.

1.2 Aravind Sundararajan, "Heat Transfer During Melt Spinning of Al-7%Si Alloy on a Cu-Be Wheel", MS Thesis, University of Illinois, December, 2007.

1.3 Sundararajan, A., and B.G. Thomas, "Heat Transfer During Melt Spinning of Al-7%Si Alloy on a Cu-Be Wheel", Cast Shop Technology, TMS Annual Meeting, Light Metals Proceedings, 2008, pp. 793-810.

Subproject 2 Comparison of computational models of turbulent fluid flow

To address the accuracy problems encountered in subproject 1, a fundamental project to quantify the accuracy of computational models of turbulent fluid flow was undertaken, to find the best computational models for engineering flow problems such as this one. In this work, several low and high Reynolds number versions of k-ε and Reynolds stress turbulence models have been evaluated in a channel and a square duct flow with and without a magnetic field by comparing the predictions with direct numerical simulations data. The simulations are performed using FLUENT solver. The additional source terms for magnetic field effects on turbulence have been included through user-defined functions. A systematic assessment of the predicted mean flow, turbulence quantities, frictional losses and computational costs of the various turbulence models is presented.

All the models predict mean axial velocity reasonably well, but the predictions of turbulence parameters are less accurate. Velocity predictions are worse for the square duct flow due to secondary flows generated by the turbulence. The implementation of the MHD sources generally improves predictions in MHD flows, especially for low-Re k-ε models. The high-Re models using the wall treatments show little improvement, perhaps due to the lack of MHD effects in the wall formulations. Finally, at low Reynolds numbers, the Lam-Bremhorst (LB) low-Re k-ε model was found to give better predictions than other models for both hydrodynamic and magnetic field influenced turbulent flows.

Sample results from the project are tabulated in Table 2.5, which compare pressure drops predicted using various turbulence models. These results show that the standard K-e model with enhanced wall treatment (RKE-EWT) overpredicts the exact DNS solutions by ~10%. The error is worse at lower Re number (near 5000), than for high Re (50,000), which explains the underprediction of the liquid puddle length in sub-project 1. Complete details of this comprehensive study are given in Ref. 2.1.

Table 2.5 Mean streamwise pressure gradient in different flows predicted by various models

| | Channel (Re=45818) | Channel (Re=4586) | Channel (Re=4710, Ha=6) Mag-Ind Method | | Square duct (Re=5466) | Square duct (Re=5602, Ha=21.2) Mag-Ind/Elec Pot Methods | |
|---|---|---|---|---|---|---|---|
| | | | With MHD sources | Without MHD sources | | With MHD sources | Without MHD sources |
| DNS | 2.0 | 2.0 | 2.0 | | 4.0 | 0.01857 | |
| RKE-EWT | 1.97 | 2.20 | - | - | 4.46 | 0.0228/0.0228 | - |
| SKE-EWT | 2.02 | 2.20 | 2.40 | 2.47 | 4.46 | - | - |
| RNG-EWT | 1.99 | 2.20 | - | - | - | - | - |
| RSM-LPS-EWT | 2.08 | 2.16 | 2.37 | 2.42 | 5.0 | 0.0244 | - |
| RKE-NWF | 1.83 | - | - | - | - | - | - |
| SKE-NWF | 1.90 | - | - | - | - | - | - |
| RNG-NEWF | 1.83 | - | - | - | - | - | - |
| RSM-LPS-NEWF | 1.84 | - | - | - | - | - | - |
| RKE-SWF | 1.85 | - | - | - | - | - | - |
| SKE-SWF | 1.94 | - | - | - | - | - | - |
| RNG-SWF | 1.89 | - | - | - | - | - | - |
| RSM-LPS-SWF | 1.85 | - | - | - | - | - | - |
| RSM-Sω | - | 1.94 | - | - | - | - | - |
| Abid | - | 2.07 | - | - | - | - | - |
| LB | - | 1.97 | 2.04 | 2.18 | 4.28 | 0.0190 | 0.0215 |

| | | | | | | | |
|---|---|---|---|---|---|---|---|
| LS | - | 3.87 | - | - | - | - | - |
| YS | - | 2.13 | - | - | - | - | - |
| AKN | - | 2.11 | - | - | - | - | - |
| CHC | - | 1.68 | - | - | - | - | - |

2.1 Chaudhary, R, B.G. Thomas and S.P. Vanka, "Evaluation of turbulence models in MHD channel and square duct flows" J. Turbulence, submitted, 2010.

Subproject 3) New method to coupled fluid flow and thermal-stress in solidification processes

A new numerical has been developed to couple the results from a fluid flow analysis into a thermal-stress code in order to efficiently simulate the coupled multiphysics of fluid flow, heat transfer, solidification, and thermal stress analysis. The new methodology involves first simulating the fluid flow in a domain that consists only of the liquid pool, using boundaries fixed at the liquidus temperature. The "superheat flux" is extracted at the boundary and is converted to an equivalent latent heat of fusion as follows:

$$\Delta H_f = \frac{q''_{superheat}}{\rho_s \, v} \qquad (1)$$

Where $\Delta H_f$ = supplement to latent heat from superheat transport in liquid pool (J/kg)

$q''_{superheat}$ = superheat flux (W/m$^2$) calculated along boundaries of flow domain, where boundary condition is fixed temperature at the liquidus temperature

$\rho_s$ = density of solidifying metal (kg/m$^3$)

$v = \frac{d\delta}{dt}$ = instantaneous solidification front velocity (m/s)

The solidification front velocity is approximated from the liquidus front position data by a simple preliminary analysis of the solidification without including the effect of fluid flow. This term could be updated for more accuracy by repeating the computation, although initial work suggests that this is not necessary for the melt-spinning process of concern in the present work.

The method has been demonstrated on two different test problems, chosen to test its limits. The first problem is simple one-dimensional solidification of a steel shell with superheat and stagnant fluid flow. The new method matches the results of a full computation that includes the liquid pool, and also matches an available analytical solution for this simple problem. The second test problem is a transient two-dimensional solidification of a ledge being impacted with a fluid jet that produces a large transverse variation in superheat flux. The new method again matches. Complete details of the new methodology are described in journal publication Ref. 3.1.

The method developed in this subproject will be particularly beneficial for more realistic thermo-mechanical modeling in continuous casting processes, such as strip casting where spatially and temporally non-uniform super heat fluxes are produced by turbulent mixing in liquid pool and can be calculated by CFD methods. The superheat flux variation has been neglected previous thermo-mechanical models of the strip casting process using commercial software such as Abaqus. The methodology was first demonstrated by applying it to a continuous casting process of a complex-shaped beam blank strand. This process was chosen because solidification front measurements were available for comparison. The new methodology matched well with the measurements, and demonstrated the

importance of this new multi-physics approach. Complete details of this application are given in journal publication Ref. 3.2.

The new Abaqus solidification models not only enable thermo-mechanically coupling, but also enable coupling with CFD software (such as Fluent) to calculate the effect of fluid flow in the liquid pool. This method will enable more accurate simulation of the phenomena for this and other solidification processes.


3.1 Koric, S., B.G. Thomas, and V. R. Voller, "Enhanced Latent Heat Method to Incorporate Superheat Effects Into Fixed-Grid Multiphysics Simulations," Numerical Heat Transfer, Part B: Fundamentals, 57:6, 396-413, 2010; http://dx.doi.org/10.1080/10407790.2010.496657.

3.2 Koric, S., L.C. Hibbeler, R. Liu, and B.G. Thomas, "Multiphysics Model of Metal Solidification on the Continuum Level," Numerical Heat Transfer, Part B: Fundamentals, 2010, in press.


Subproject 4) Explicit Coupled Thermo-Mechanical Finite-Element Model of Steel Solidification

A new method to simulate thermal-stress evolution has been developed. It is described in a paper that recently appeared in Int. J. Num. Meths. In Eng. which is attached to this report. The explicit finite-element method is applied in this work to simulate the coupled and highly-nonlinear thermo-mechanical phenomena that occur during molten metal solidification in continuous casting processes. Variable mass scaling is used to efficiently model these processes in their natural time scale using a Lagrangian formulation. An efficient and robust local-global viscoplastic integration scheme [4.1] to solve the highly temperature- and rate-dependent elastic-viscoplastic constitutive equations of solidifying steel has been implemented into the commercial software ABAQUS/Explicit [4.2] using a VUMAT subroutine. The model is first verified with a known semi-analytical solution from Weiner and Boley [4.3]. It is then applied to simulate temperature and stress development in solidifying shell sections in continuous casting molds using realistic temperature-dependent properties and including the effects of ferrostatic pressure, narrow face taper, and mechanical contact. Example simulations include a fully-coupled thermo-mechanical analysis of a billet casting and thin-slab casting in a funnel mold. Explicit temperature and stress results are compared with the results of an implicit formulation and computing times are benchmarked for different problem sizes and different numbers of processor cores. The explicit formulation exhibits significant advantages for this class of contact-solidification problems, especially with large domains on the latest parallel computing platforms.


[4.1] Koric, S., and B.G. Thomas. Efficient Thermo-Mechanical Model for Solidification Processes. *International Journal for Num. Methods in Eng* 2006; 66:1955-1989.

[4.2] *ABAQUS User Manuals v6.7.* Simulia Inc. 2007.

[4.3] Weiner JH and Boley BA. Elastic-plastic thermal stresses in a solidifying body. *J. Mech. Phys. Solids* 1963;11:145-154.


Subproject 5) Simulation of Effect of air pockets on pit formation in single-roll spin-casting of aluminum

The following hypothesis has been developed to explain the observation of holes or pits in the solidified aluminum strip product from the single-roll spin-casting process.

1) Air pockets can be entrapped at the meniscus at the start of the process. These air pockets slow down solidification, due to their low thermal conductivity.
2) This keeps the metal molten in the local region near the bubble during the entire process, even after the surrounding metal has solidified into strip.
3) Due to surface tension of the remaining liquid, a smooth, round hole is formed at the prior location of each air pocket, if it has a critical size to prevent solidification from bridging across the liquid pocket before the strip exits the liquid pool and becomes starved for liquid metal.

A computational model (developed in our previous NSF project) was applied to investigate this hypothesis. Strip solidification has been predicted at different wheel rotation speeds in the presence of air pockets of different sizes. For each rotation speed, the critical sizes of gas pocket that just prevent solidification are extracted from the results. The results seem plausible. The next step is to compare with experiments conducted at Cornell to confirm if this model (and corresponding hypothesis) is correct or not.

A computational model is applied to investigate this hypothesis. Strip solidification is predicted at different wheel rotation speeds in the presence of air pockets of different sizes. For each rotation speed, the critical sizes of gas pocket that just prevent solidification are extracted from the results.

Fig. 5.1 shows the growth of the solidified shell with time (distance along the wheel from the initial contact point at the meniscus).

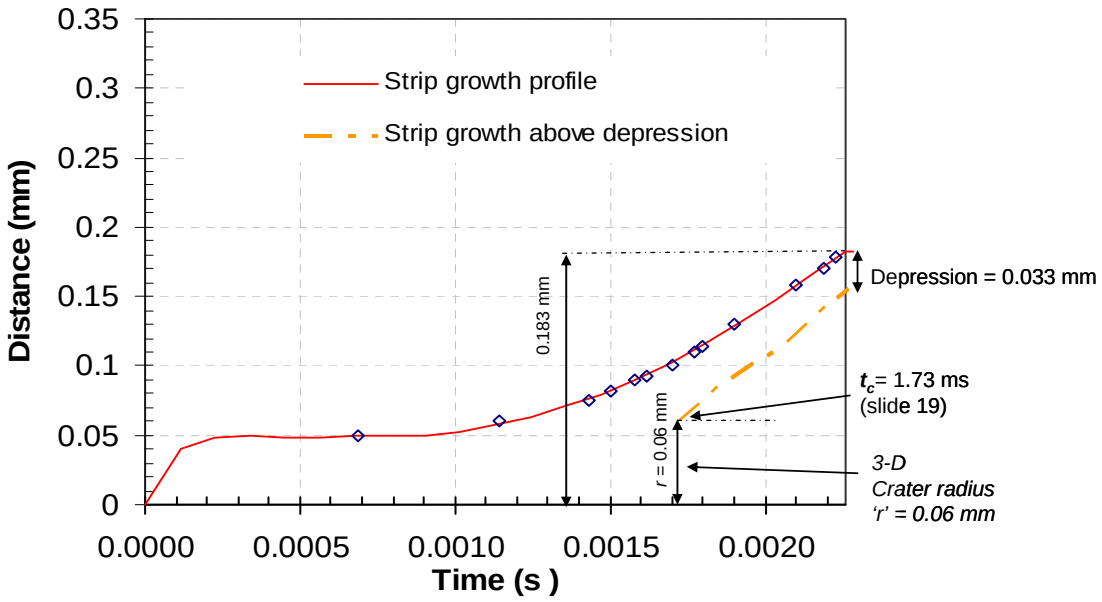


Fig. 5.1 Strip growth with time from the contact meniscus, comparing local thickness at the gas pocket with thickness elsewhere. The critical time (1.73ms in this case) indicates the puddle length that just barely produces a pit (for the given wheel speed). Longer times produce a depression (with very thin solid layer above the dimple-depression). Knowing the relation between puddle length and wheel speed, this time indicates a critical wheel speed where the puddle length is reached in exactly this time.

The model was run to find the critical wheel speed for pit formation for a variety of different pit sizes (indicated by the "crater radius") The results are given in Fig. 5.2 with the corresponding strip thickness.

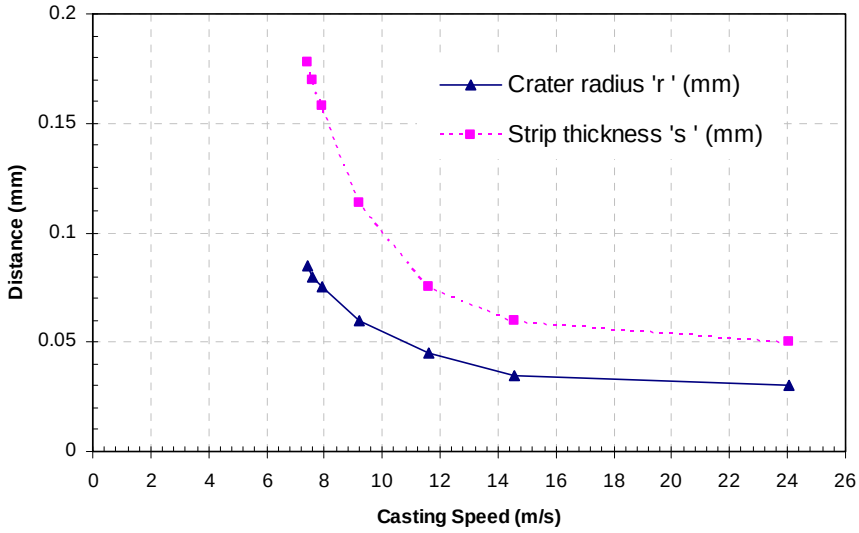


Fig. 5.2 Effect of wheel speed on strip thickness and critical gas pocket size that causes pit formation.

## Strip Cutting Study

Via the same mechanism as pit formation, a row of dimples from bubbles captured at the meniscus can retard solidification so much that the strip does not completely solidify across the entire width. After exiting the puddle region, the strip would be effectively cut into 2 pieces. The critical size and spacing of dimples needed achieve this cutting effect has been studied.

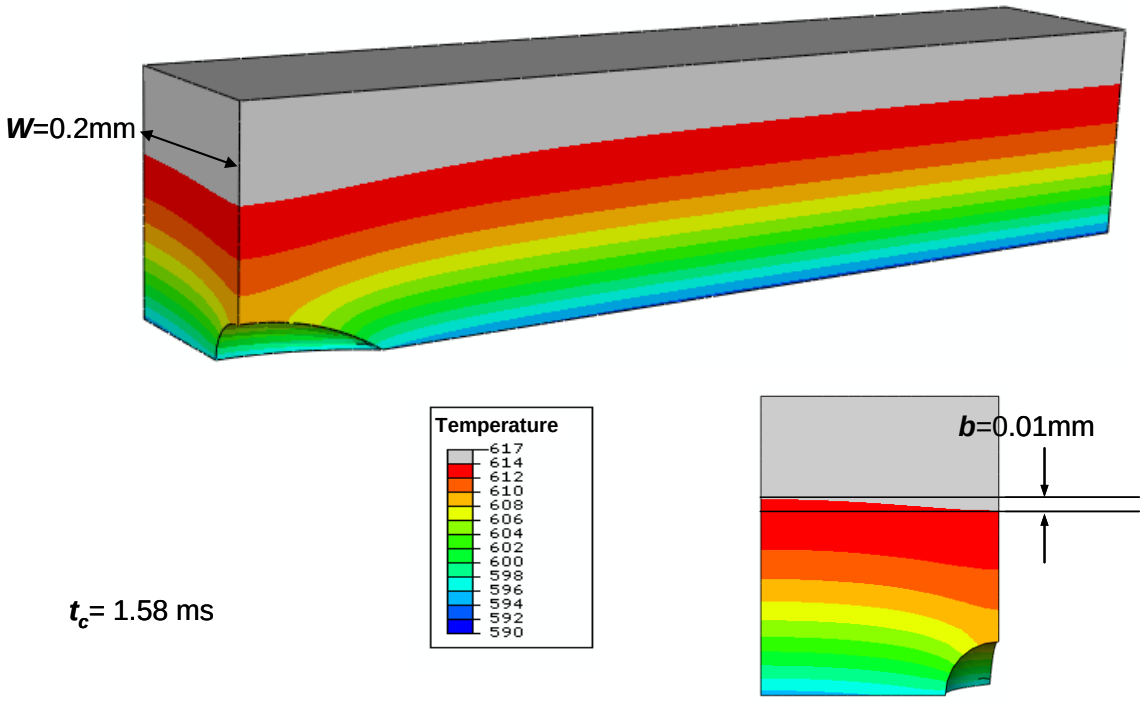


Fig. 5.3. Elongated dimple depression and its effect on depression formation across the strip. Note the variation in depression depth is only 0.01mm (over 0.2mm dimple spacing), which is small compared with the depression variation along the length. Thus, the row of dimples produces a transverse depression.

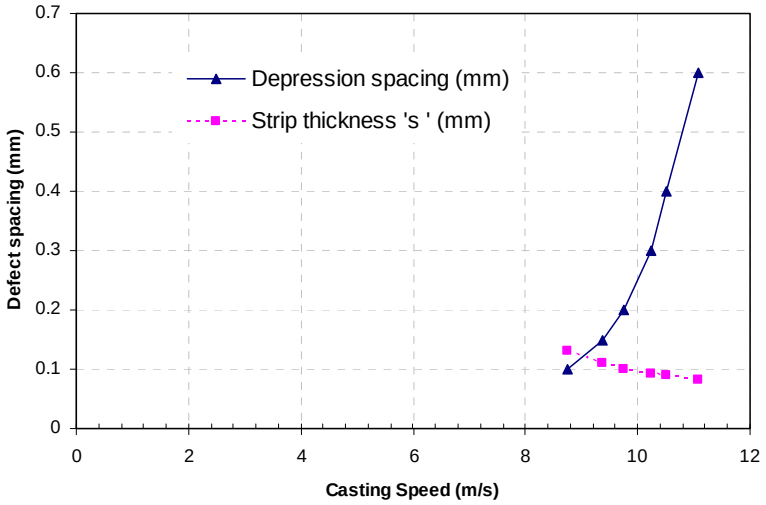


Fig. 5.4. Critical distance between gas pockets that leads to a continuous linear void across of the strip, cutting it into separate pieces. Increasing speed makes the strip thinner, so gap formation is easier: thus, the critical spacing between gas pockets is larger at higher speed.